Diffusion Coefficient of Fluorescein-labeled Tubulin in the Cytoplasm of Embryonic Cells of a Sea Urchin: Video Image Analysis of Fluorescence Redistribution after Photobleaching

E. D. SALMON, W. M. SAXTON, R. J. LESLIE, M. L. KAROW, and J. R. McINTOSH
Department of Biology, University of North Carolina, Chapel Hill, North Carolina 27514; and Department of Molecular, Cellular, and Developmental Biology, University of Colorado, Boulder 80309

ABSTRACT The diffusion coefficient of tubulin has been measured in the cytoplasm of eggs and embryos of the sea urchin *Lytechinus variegatus*. We have used brain tubulin, conjugated to dichlorotriazinyl-aminofluorescein, to inject eggs and embryos. The resulting distributions of fluorescence were perturbed by bleaching with a microbeam of light from the 488-nm line of an argon ion laser. Fluorescence redistribution after photobleaching was monitored with a sensitive video camera and photography of the television-generated image. With standard photometric methods, we have calibrated this recording system and measured the rates of fluorescence redistribution for tubulin, conjugated to dichlorotriazinyl-aminofluorescein, not incorporated into the mitotic spindle. The diffusion coefficient (D) was calculated from these data using Fick's second law of diffusion and a digital method for analysis of the photometric curves. We have tested our method by determining D for bovine serum albumin (BSA) under conditions where the value is already known and by measuring D for fluorescein-labeled BSA in sea urchin eggs with a standard apparatus for monitoring fluorescence redistribution after photobleaching. The values agree to within experimental error. $D_{\text{tubulin}}^{\text{cytoplasm}} = 5.9 \pm 2.2 \times 10^{-8}$ cm^2/s; $D_{\text{BSA}}^{\text{cytoplasm}} = 8.6 \pm 2.0 \times 10^{-8}$ cm^2/s. Because $D_{\text{BSA}}^{\text{H}_2\text{O}} = 68 \times 10^{-8}$ cm^2/s, these data suggest that the viscosity of sea urchin cytoplasm for protein is about eight times that of water and that most of the tubulin of the sea urchin cytoplasm exists as a dimer or small oligomer, which is unbound to structures that would impede its diffusion. Values and limitations of our method are discussed, and we draw attention to both the variations in D for single proteins in different cells and the importance of D for the upper limit to the rates of polymerization reactions.

There are several theories about the mechanisms of spindle and cytoplasmic microtubule assembly (1–8), but the actual pathways of tubulin subunit exchange between polymer and subunit pools are not yet understood. To understand microtubule assembly in vivo, one would like to know the rate constants for subunit association in cells. This rate of association is the product of the concentration of tubulin in equilibrium with the microtubules, the number of exchange sites per microtubule, and the bimolecular rate constant for tubulin assembly in the living cell (6, 8). The assembly rate constants have been measured for the end-dependent, nucleated condensation polymerization of tubulin and associated proteins that occurs in vitro (reviewed in reference 8). However, the magnitude of the association rate constant depends directly on the diffusion coefficient (9, 10), so the use of in vitro association rate constants in the analysis of tubulin assembly for mitotic spindles in vivo (8) depends on the relative magnitudes of the diffusion coefficients of tubulin in the two situations. In this article we present data on the diffusion coefficient of a soluble, fluorescently labeled tubulin injected into the cytoplasm of embryonic sea urchin cells. By using techniques of fluorescent analog cytochemistry (11, 12) and a new method based on video image analysis, we have measured the mobility of fluorescent tubulin from measurements of fluorescence redistribution after laser photobleaching (FRAP)[1] of localized regions of the cytoplasm (13–15). A low light-level video camera was used to record the distribution

[1] Abbreviations used in this paper: DTAF, dichlorotriazinyl-aminofluorescein; FITC, fluorescein isothiocyanate; FRAP, fluorescence redistribution after photobleaching.

THE JOURNAL OF CELL BIOLOGY · VOLUME 99 DECEMBER 1984 2157-2164

of fluorescence in the specimen, and images from a video monitor were recorded on photographic film. The diffusion constant was calculated by a numerical analysis, based on Fick's second law of diffusion, using the recovery profiles of fluorescence at various times after photobleaching. We calibrated the method with fluorescein-tagged BSA in solutions of various concentrations of glycerol (16). Our measured value of $D_{tubulin}^{cytoplasm}$ is compared here with values for other proteins in various cell types and used elsewhere in analysis of tubulin assembly pathways (8).

MATERIALS AND METHODS

Reagents: Microtubule protein was purified from beef brain (17) and tubulin was labeled with dichlorotriazinyl-aminofluorescein (DTAF) from Research Organics, Cleveland, OH, as described by Keith et al. (18), with some modifications (19). For some experiments the DTAF-tubulin (dimer mol wt ≃ 110,000) was purified by phosphocellulose chromatography (18). In other experiments, DTAF-tubulin was purified by cycles of assembly in 1 M glutamate (19). Protein prepared by either method gave similar results. The average molar ratio of dye-to-protein was ~0.4 for the phosphocellulose purified tubulin based on an extinction coefficient for DTAF of 27,000, the value we measured in tubulin assembly buffer. For phosphocellulose-purified DTAF-tubulin, ~10–15% of the fluorescence migrated at the dye front on SDS PAGE, while there was little fluorescence at the dye front with the glutamate procedure (19). Both preparations, however, yielded equivalent diffusion constants, indicating that the DTAF seen at the dye front in SDS PAGE is tightly associated with the tubulin under nondenaturing conditions. The DTAF-tubulin stocks were stored at 2–4 mg/ml as 10-μl samples in liquid N_2. Fluorescein isothiocyanate-labeled BSA (FITC-BSA), mol wt ≃ 68,000, the generous gift of Michael Zavortink, had a dye-to-protein ratio of ~2. It was stored at −20°C as a 4 mg/ml stock in 10 mM PO_4, pH 7.0 buffer.

Injection of Eggs and Embryos: Eggs and embryos of *L. variegatus* were cultured in a Kiehart–Ellis "wedge" chamber (20) as described by Salmon et al. (8). The wedge chamber flattens these 115-μm-diam cells to ~75 μm in the dimension parallel to the microscope optic axis. About 0.5 h before injection, a 10-μl stock of DTAF-tubulin was thawed, dialyzed into injection buffer (20 mM Na-glutamate, pH 6.8, 1 mM $MgCl_2$, 1 mM EGTA, 0.5 mM GTP) at 4°C, and stored on ice. For FITC-BSA injections, the stock solution was diluted 1:8 into injection buffer. Injections into living cells were performed using standard glass-needle procedures (21), modified for sea urchin embryos. The outside diameters of the needle tips were 0.5–1 μm. Between 15 and 40 embryos were injected ~15 min after fertilization. Injection volumes were estimated from the diameter of the bolus of injected fluid immediately after injection. From these numbers and the dimensions of the unflattened egg, we estimate that the volume of our injected samples ranged from 1 to 3% of the total cell volume.

Calibration Chambers: We calibrated our diffusion coefficient measurements using a 4 mg/ml FITC-BSA stock diluted 1:400 into distilled water mixed with various amounts of glycerol. These solutions were sealed between a 22 × 22 coverslip and a slide; the coverslip was held above the slide by the 75-μm thickness of Scotch double-stick transparent tape (3M Company, Minneapolis, MN). This thickness approximated the thickness of a cell in the Kiehart–Ellis wedge chamber.

Fluorescence Microscopy, Photobleaching, and Video Recording: Fluorescence microscopy was performed using a Zeiss Universal microscope equipped with Zeiss fluorescein filters, epi-fluorescence optics, HBO 200-W mercury burner, and a 25×/NA = 0.50 Zeiss Neofluor phase objective as diagrammed in Fig. 1 (Carl Zeiss, Inc., New York). The primary image was projected at about ×4 magnification onto the first photocathode of a Venus DV-2 low light-level video camera (Farmingdale, NY). Video images from a 9-in monitor (usually a Conrac SNA9, Corvinia, CA) were recorded by 0.5-s exposures on Kodak Plus-X 35 mm film (Eastman Kodak Co., Rochester, NY) with a Nikon FM camera (Nikon Inc., Garden City, NY) at about f/11. Film was developed in HC110, dilution B, for 5 min at 22°C. The Venus DV-2 camera was operated at full manual gain and with a constant setting of the pedestal control for all the experiments. Monitor settings for brightness and contrast were kept constant. For photobleaching, a laser beam was focused on the aerial image plane of the epi-illuminator using a Spectra-Physics (Mountain View, CA) 1-in beam-expanding telescope set to a focal length of ~110 cm. A 90% reflecting, front-silvered mirror mounted in the epi-illuminator near the microscope was used both to make the laser beam and the microscope illumination coaxial and to reduce the intensity of the illuminating beam (Fig. 1).

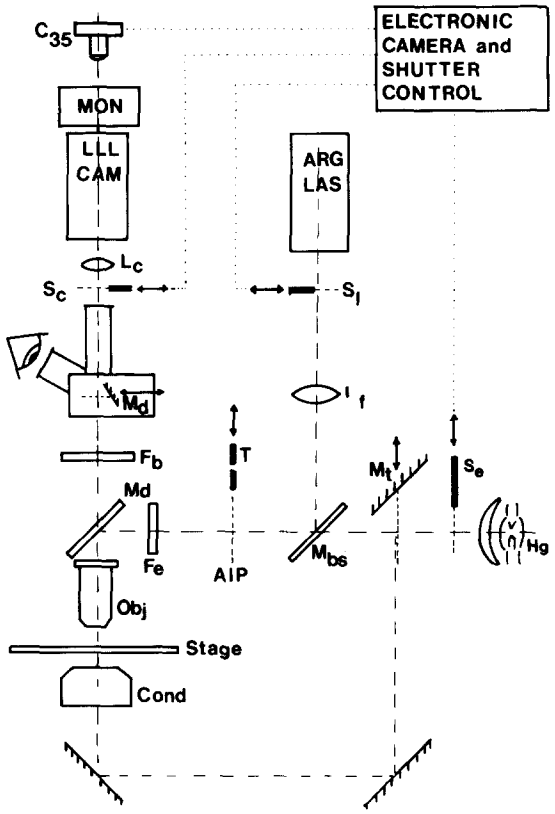

FIGURE 1 Optical pathways for fluorescence microscopy, laser photobleaching, and video recording. Major components are described in the text. Symbols are as follows: *Hg*, 200-W mercury burner; S_e, epi-illuminator shutter; M_t, mirror for switching between trans- or epi-illumination; M_{bs}, beam-splitting mirror, reflecting ~20% of laser illumination; *ARG LAS*, laser, usually argon ion; S_l, laser beam shutter; L_f, lens focusing laser at AIP; *AIP*, aerial image plane conjugate with specimen plane; F_e, fluorescence excitation filters; F_b, fluorescence barrier filters; M_d, dichroic mirror; *Cond*, condenser; *Obj*, objective; M_d, beam director to either oculars or video camera; S_c, camera shutter; L_c, camera projection lens; *LLL CAM*, low light level video camera; *MON*, video monitor; C_{35}, 35-mm camera with motor drive.

With the ×25 objective, the waist of the focused laser beam at the specimen plane was slightly asymmetrical, varying from 12 to 14 μm in diameter, as measured from photographs of the fluorescence produced by focusing the beam on double-stick Scotch tape.

Electronic shutters gated the various light paths of the system (Fig. 1). A Zeiss shutter mounted between the HBO 200 and the epi-illuminator shielded the specimen from prolonged illumination. This shutter was opened and closed by an electronic controller designed and fabricated by Hannaway and Associates, Boulder, CO. The controller used timing pulses from the Venus camera to synchronize shutter activity with the initiation of video frames. The same controller fired the shutter of the Nikon camera, which recorded the video images from a monitor after a delay of two video frames (1/15 s) necessary to allow stabilization of the video electronics after the rapid increase in light intensity brought on by opening the specimen-shielding shutter. A second pair of shutters controlled the irradiation of the specimen by the laser. A 6-mm-diam electronic shutter with front-aluminized leaves (Vincent Associates, Rochester, NY, model 225L plus driver) controlled the laser beam irradiation of the specimen. An additional shutter (25-mm diam, Vincent Associates, model 225L plus driver) was mounted in front of the video camera. This shutter was usually open, but closed during laser photobleaching to prevent damage to the photocathode of the Venus camera. These two shutters were controlled by a homemade timer, which allowed both individual and gang operation for exposures ranging from 10 ms to 10 s.

During these experiments, three different lasers were used (see acknowledgments). Their beam powers ranged from 15 to 100 mW. Two air-cooled argon lasers were operated at their 488-nm line while a He-Cd laser was operated at

442 nm. Photobleaching times varied from 2 to 8 s.

In a typical experiment, our procedure was as follows: (*a*) The location of the focused laser beam, attenuated by a 3 OD neutral-density filter, was marked on the video monitor by the location of the laser beam fluorescence on a piece of double-stick Scotch tape. (*b*) Under epi-illumination from the HBO 200-W lamp, which was attenuated to minimize photobleaching, the specimen was positioned with respect to the mark on the monitor and brought to focus. (*c*) Whole-field epi-illumination was used to record a 0.5-s exposure of the specimen field through the video camera onto 35-mm film before bleaching. (*d*) Photobleaching was performed with the full power of the laser. (*e*) By using full-field epi-illumination with dim light, we made photographic recordings within 1 s after completion of the photobleach and at ensuing intervals to record recovery. We have shown that the bleaching introduced by the illumination necessary for recording with video photography was negligible so long as no more than ten 0.5-s photographs of the video monitor were made.

Fluorescence Intensity vs. Film Density: In our image-recording scheme, light intensity at the specimen plane (I_s) is converted to optical density on the 35-mm film (OD_f) photographed from the monitor. The Venus DV-2 low light-level camera uses a vidicon tube with two "generation 1" image intensifiers at the input. Like film, the vidicon tube is a logarithmic detector of light, gamma $\simeq$ 0.7. We determined the relation between OD_f and I_s with a demagnified photograph (1 × 10 mm) of a standard Kodak transparent grey scale. The grey scale was placed on the field diaphragm of the microscope beneath a Zeiss IV, NA = 1.4, trans-illumination condenser. The grey scale was illuminated by 546-nm light passing through an interference filter that had a 15-nm bandwidth. A ×16/NA = 0.33 Zeiss Plan objective was used to produce an image of the grey scale on the video monitor where it was photographed with the 35-mm camera. The Venus camera and monitor controls were set as for the photobleaching experiments. Transillumination of the specimen field by Kohler illumination gives nearly uniform intensity across the central field of view in the microscope, but an image of the specimen field without the grey scale was recorded as a control for uneven illumination, vignetting, and shading in the camera. Negatives were scanned using a Joyce–Loebl (model 3C) microdensitometer. The cross section of the measurement beam was adjusted to be equivalent to a 2 × 4 μm rectangle at cellular dimensions. The long axis of the measurement beam was normal to the scan direction. The optical density of the image of the wedge negative was corrected for shading and uneven illumination, then plotted against the corresponding optical density steps in the original grey scale as shown in Fig. 2.

Light intensity through the optical density wedge is given by:

$$\log I/I_{ill} = -OD_{gs}, \tag{1}$$

where I is the light intensity at a step along the grey scale wedge with a given optical density (OD_{gs}), and I_{ill} is the intensity of the light illuminating the grey scale. As seen in Fig. 2, the change in OD_f for the negative image photographed from the video monitor is proportional to the negative change in OD_{gs} over at least a 0.9 OD_{gs} range. Within this range the reciprocal of the slope of the line through the data gives the log of the ratio of two specimen light intensities, I_{s2}/I_{s1}, as

$$\log(I_{s2}/I_{s1}) = TF(OD_{f2} - OD_{f1}), \tag{2}$$

where TF is the transfer coefficient of the measurement system. Because Fig. 2 is a log–log plot, the calibration curve is not expected to intercept at the origin. $OD_f = 0$ represents the unexposed optical density of the film. Values of TF ranged between 0.375 and 0.5, depending on the type of monitor used. Because TF is less than 1, contrast in the photographic negative is greater than contrast in the corresponding specimen intensity distribution.

Numerical Analysis of Optical Density Profiles: Diffusion coefficients were calculated by numerical analysis of prebleach and recovery optical density profiles scanned along the same direction through the center of the bleached region. This procedure is described in Results and the legend for Fig. 5. The Cartesian coordinates of points along an optical density profile were digitized into an Apple II Plus computer (Apple Computer, Inc., Cupertino, CA) using a Houston Instruments Hi-Pad digitizer (Austin, TX).

RESULTS AND ANALYSIS

FRAP of Eggs and Embryos

Unfertilized eggs and first division mitotic cells were photobleached for 4–8 s with a focused laser beam of waist diameter 13 ± 1 μm. Examples of bleaching and of subsequent fluorescence redistribution are shown in Fig. 3*a* for an unfertilized egg and in Fig. 3*b* for a first mitotic cell. Fig. 4 illustrates

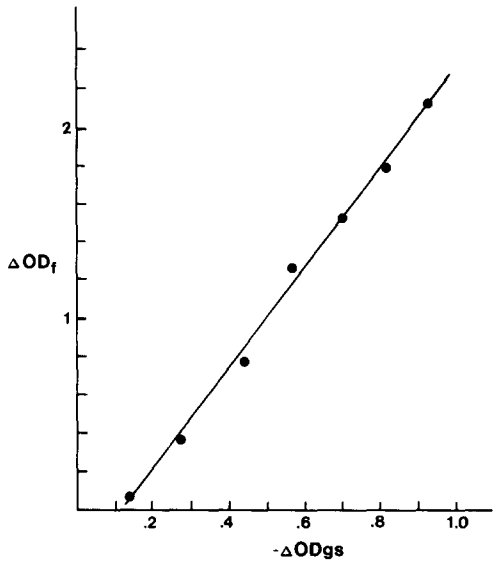

FIGURE 2 The change in film optical density (OD_f) of photographic exposures taken of a video monitor when the optical density calibration grey scale (OD_{gs}) is projected into the specimen field of the microscope. Data were taken and analyzed as described in the text.

the changes in the fluorescence profiles after bleaching, measured by optical density line scans through the center of the bleached region on the photographic negatives. In this example, photographs of the video monitor were taken 3 s before, 1 s after, and then at various subsequent times using the cell shown in Fig. 3*b*. After 20–30 s the fluorescence distribution becomes nearly uniform, but the bleaching caused by the short, intense laser pulse and the repeated dim epi-illuminations for photography has reduced the total fluorescence by ~10%.

Considerable redistribution of fluorescence occurs during the 8-s period of bleaching. The apparent diameter of the bleached region 1 s after bleaching is two to three times greater than the waist diameter of the focused laser beam (Fig. 3). For shorter bleaching times, smaller-diameter bleached spots were formed, but the extent of fluorescence bleaching was less. The electronic noise in the video system corresponded to ±0.05 OD on the film negatives. This noise limits the accuracy of fluorescence intensity measurements in our video-film recording system, so quantitating the recovery of small, short bleaches was not possible. Without a more intense laser light source, bleaching periods <4 s did not give sufficient gradients in fluorescence intensity to yield accurate results in the diffusion coefficient (D) analysis. However, our method for analyzing the redistribution of fluorescence does not depend on short bleach times. We have used an approach that allows us to determine D from bleaches with approximate cylindrical symmetry, regardless of the duration of the bleach relative to the time for subsequent fluorescence redistribution.

Analysis Procedures for Determination of Diffusion Coefficients

The magnitude of the diffusion coefficient (D) in the sea urchin cell cytoplasm can be calculated from the fluorescence intensity redistribution profiles through the center of the bleached region (Fig. 4). For this analysis, we assume that

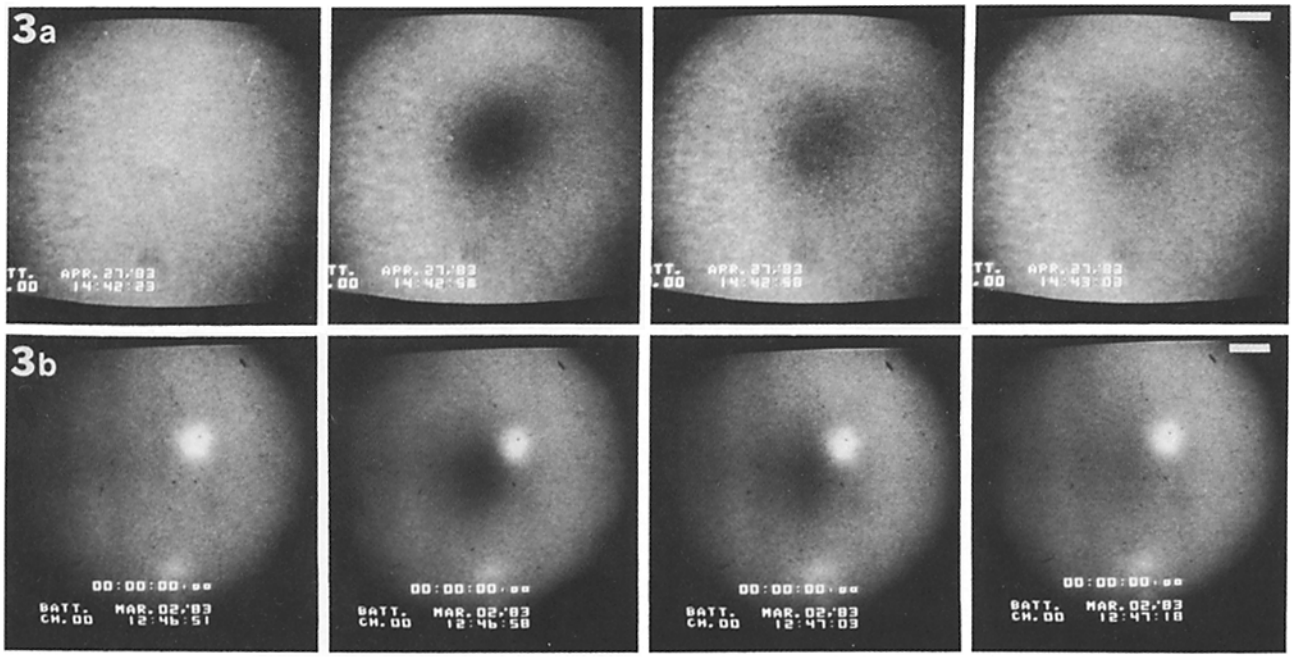

FIGURE 3 Photographs of the fluorescence distribution of an unfertilized egg (*a*) and first division embryo (*b*) before and during recovery following laser photobleaching of a central, cytolasmic region. Time, hours:minutes:seconds, is given in each frame by a video time-date generator in series between the low-light-level Venus DV-2 video camera and the video monitor. The cell in *a* was photobleached for 8 s. Bleaching ended at 14:42:49. The cell in *b* was photobleached for 4 s. Bleaching ended at 12:46:57. Bar, 20 μm. × 275.

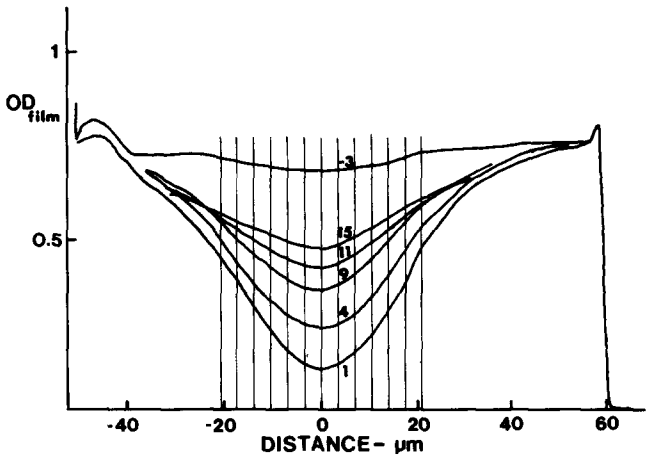

FIGURE 4 Optical density profiles through the center of a bleached region obtained by scanning the photographic negatives from the experiment shown in Fig. 3*b*. The horizontal scale has been converted to microns in the specimen plane using a scale factor derived from photographs of a microscope stage micrometer. The profiles were traced from the original Joyce-Loebl optical density scans. The profile lines were drawn by eye averaging noise fluctuation in the original data, which was usually $<\pm 0.05$ OD. Fiduciary marks for aligning successive negatives were provided by the image of the numerals of the time-date generator and the optical density or fog level of the region of the negative film adjacent to the photographic frame. A 2.0 OD wedge was used in the Joyce-Loebl to obtain the original scans. The vertical lines, parallel to the axis of symmetry through the bleached region, represent multiple, unit, radial distances away from the axis of symmetry. Optical densities along each profile curve at these unit radial distances were digitized into a computer for calculation of diffusion coefficients as described in Fig. 5 and in the text.

(*a*) the bleached region is cylindrically symmetrical about the axis of the laser beam, and (*b*) bleaching does not vary along the axis of symmetry so that axial diffusion can be neglected. In this article we have also assumed that cytoplasm is both homogeneous and isotropic, but an advantage of our approach is that these restrictions could be removed. With these assumptions, diffusion of DTAF-tubulin into the bleached region is radial in two dimensions. The concentration of unbleached DTAF-tubulin is then only a function of the time t and of the radius, r, from the axis of symmetry of the bleach. Fick's second law of diffusion becomes:

$$\partial C(r, t)/\partial t = D\frac{\partial^2 C(r, t)}{\partial^2 r} + \frac{1}{r}\frac{\partial C(r, t)}{\partial r}, \qquad (3)$$

where $C(r, t)$ is the concentration of tubulin in molecules/cm^3 at time, t, and radius, r (22, 23). The fluorescence intensity of DTAF-tubulin, $F(r, t)$ is given by:

$$F(r, t) = \alpha C(r, t) I_{ep}, \qquad (4)$$

where α is a proportionality constant related to objective numerical aperture, objective depth of field, and the cell thickness (14). I_{ep} is the intensity of the epi-illumination in the specimen field. Because $F(r, t)$ is proportional to $C(r, t)$, Eq. 3 can be written as:

$$\frac{\partial F(r, t)}{\partial t} = D\frac{\partial^2 F(r, t)}{\partial r^2} + \frac{1}{r}\frac{\partial F(r, t)}{\partial r}. \qquad (5)$$

The diffusion constant for DTAF-tubulin in the sea urchin cytoplasm was calculated from Eq. 5 by numerical analysis of the distributions of fluorescence using optical density re-

covery profiles similar to those in Fig. 4. For each profile (i) of optical density at time (t_i) in seconds after photobleaching, the ordinate position, $y(r_m, t_i)$ measured in millimeters, was digitized into a computer at multiple radial distances, r_m, measured from the axis of symmetry. Δr equals a unit of radial distance. To correct for shading in the camera and uneven epi-illumination, radial points along the prebleached (p) profile, $y(r_m, p)$, were also digitized. For each r_m, fluorescence intensity normalized by the prebleach magnitude, $NF(r_m, t_i)$, is calculated from Eq. 2 by:

$$NF(r_m, t_i) = \log^{-1}[y(r_m, t_i) - y(r_m, p) \times SF \times TF], \quad (6)$$

where SF is the scale factor in OD_f/millimeter and TF is the proportionality constant relating logarithmic changes in light intensity to OD_f (see Eq. 2 and Fig. 2).

At a radial distance ($r_m + 0.5\Delta r$), the average diffusion constant, $D(r_m, t_i)$, is calculated from Eq. 5. The derivatives of fluorescence with respect to time may be approximated from two sequential, relative fluorescence recovery profiles. The derivatives with respect to r are determined from each profile relating fluorescence to position. The scheme using four radial points for numerical analysis is illustrated in Fig. 5 for positive values of r_m. The relevant equations are shown below.

$$D(r_m, t_i) = DF(r_m, t_i)/(SD(r_m, t_i) + FD(r_m, t_i)), \quad (7)$$

where

$$DF(r_m, t_i) = \frac{NF(r_m, t_{i+1}) - NF(r_m, t_i) + NF(r_{m+1}, t_{i+1}) - NF(r_{m+1}, t_i)}{2(t_{i+1} - t_i)}; \quad (8)$$

$$SD(r_m, t_i) = \frac{0.66(NF(r_{m+2}, t_i) - NF(r_m, t_i) + NF(r_{m-1}, t_i) - NF(r_{m+1}, t_i))}{2\Delta r^2} + \frac{0.33(NF(r_{m+2}, t_{i+1}) - NF(r_m, t_{i+1}) + NF(r_{m-1}, t_{i+1}) - NF(r_{m+1}, t_{i+1}))}{2\Delta r^2}; \quad (9)$$

$$FD(r_m, t_i) = \frac{0.66(NF(r_{m+2}, t_i) - NF(r_m, t_i))}{2\Delta r(r_m + 0.5\Delta r)} + \frac{0.33(NF(r_{m+2}, t_{i+1}) - NF(r_m, t_{i+1}))}{2\Delta r(r_m + 0.5\Delta r)}. \quad (10)$$

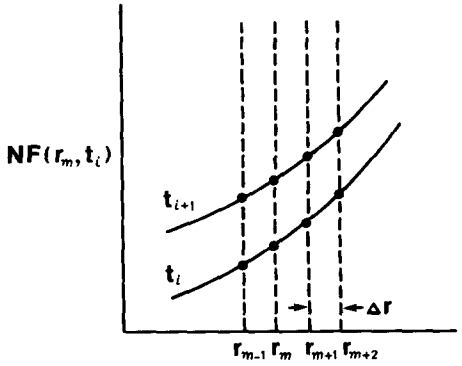

FIGURE 5 Sketch of the data points used for the calculation of the diffusion coefficient, $D(r_m, t_i)$ for a unit volume bounded by r_m and r_{m+1} and centered at $r_m + r/2$. For details, see text.

$D(r_m, t_i)$ is calculated at different radii (by letting m vary from 1 to MM, where MM is the highest value of the index m) and at different times (by letting i vary from 1 to $IM - 1$, where IM is the maximum value of the index i. The useful values of $D(r_m, t_i)$ are then averaged to give the best estimate of D. A sample computer printout is shown in Fig. 6, which is the analysis of the experiment shown in Figs. 3 and 4. For negative values of r_m, Eqs. 7–10 must be appropriately modified to match the scheme shown in Fig. 5. Because the slopes of the recovery curves are small, the calculated diffusion coefficients for later recovery times or large radial distances can vary considerably from the average value. Values of D from the edges of the bleach were discarded in calculating average values for the diffusion coefficient. Note also that with this method, values for the diffusion coefficient cannot be calculated from the data at $r = 0$.

Calibration

The numerical accuracy of our video image analysis method was initially tested by calculating diffusion coefficients from published concentration profiles of diffusion experiments. Concentration distributions for various times during inward cylindrical diffusion are plotted by Crank (22, Fig. 5.3) and by Carslaw and Jaeger (23, Fig. 24). For a given value of $D = 5 \times 10^{-8}$ cm^2/s, our graphical method yielded $D = 4 \pm 2 \times 10^{-8}$ cm^2/s. Distortions in the published curves may account for this small difference between our measured value and the expected value of D. We experimented with different radial distances over which we could obtain average values for the differentials in Eq. 5. The four-radial-point scheme shown in Fig. 5 and given by Eqs. 7–10 was the most accurate and least sensitive to noise irregularities in the profile tracings.

Final calibration of the method was obtained by measuring values of the diffusion coefficients for FITC-BSA in various glycerol/H_2O solutions (16). These measured values are compared in Fig. 7 to the value of the diffusion constant predicted from the Stokes'-Einstein diffusion equation, the viscosity of the glycerol solutions, and the published diffusion coefficient for BSA in aqueous media, $D^{20°}_{BSA} = 68 \times 10^{-8}$ cm^2/s (24, 25). From the Stokes'-Einstein equation (13),

$$D = kT/6\eta a, \quad (11)$$

and

$$D_2/D_1 = (T_2\eta_1/T_1\eta_2)(MW_1/MW_2)^{1/3}, \quad (12)$$

where k is Boltzman's constant, T is temperature in °K, η is the coefficient of viscosity, and a is the equivalent spherical radius of the particle. To a first approximation, the radius a is proportional to the cube root of the particle molecular weight, MW. $D^{25°}_{BSA}$ was calculated from Eq. 12 using the known value of $D^{20°}_{BSA}$ and values of η obtained from the Handbook of Chemistry and Physics (26) for the glycerol solutions and corrected for $T = 25$°C. The application of the Stokes'-Einstein equation is a first approximation, in that η is quite temperature-sensitive at higher glycerol concentrations. Further, hydration effects on the radius, a, have been ignored (16). This analysis (Fig. 7) does demonstrate, however, that our image analysis method for measurement of the diffusion coefficient is accurate to within 10–60% over the range of diffusion coefficient values between 15 and 0.3×10^{-8} cm^2/s, the range of diffusion constant values reported for FITC-BSA in living cells (25, 27, 28).

Listing of parameters:

Number of line scans = 7
Number of data points/line = 13
Y scale factor = 0.0101 OD/mm
X scale factor = 0.69 μm/mm
Delta r = 3.4615 μm
Transfer factor, TF = 0.5
Starting m value, ms = 3

Average $D = 9.5 \times 10^{-8}$ cm²/s
Average SD = 3.86×10^{-8} cm²/s

Times, t_i, and average diffusion coefficients, D_i, per line scan:

t_i (s)	$D_i \pm SD_i$ ($\times 10^{+8}$ cm²/s)
1	11.45 ± 2.15
4	13.59 ± 3.21
6	9.34 ± 3.21
9	9.31 ± 2.5
11	4.91 ± 0.86
15	8.41 ± 2.18

Listing of NF (i, m)/D (i, m) for t_i and r_m)

	i = 1	2	3	4	5	6	7
m	r_m (μm)	NF (1, m) / D (1, m)	NF (2, m) / D (2, m)	NF (3, m) / D (3, m)	NF (4, m) / D (4, m)	NF (5, m) / D (5, m)	NF (6, m) / D (6, m)	NF (7, m) / D (7, m)
1	−20.8	0.71	0.76	0.78	0.8	0.82	0.81	0.82
		0	0	0	0	0	0	0
2	−17.3	0.66	0.71	0.74	0.77	0.79	0.79	0.81
		0	0	0	0	0	0	0
3	−13.8	0.61	0.66	0.7	0.73	0.75	0.77	0.8
		11.92	13.43	9.44	10.99	5.15	11.82	0
4	−10.4	0.57	0.63	0.67	0.71	0.73	0.75	0.79
		8.93	10.51	7.87	8.72	4.85	7.22	0
5	−6.9	0.54	0.61	0.64	0.69	0.7	0.74	0.78
		9.81	10.62	7.43	6.49	4.26	6.96	0
6	−3.5	0.52	0.59	0.63	0.67	0.7	0.73	0.78
		10.63	11.92	8.21	6.66	5.03	9.11	0
7	0	0.51	0.59	0.63	0.67	0.7	0.73	0.78
	0	0	0	0	0	0	0	0
8	3.5	0.52	0.6	0.64	0.68	0.71	0.73	0.79
		10.9	10.29	5.21	6.33	2.96	4.67	0
9	6.9	0.53	0.61	0.66	0.7	0.73	0.75	0.8
		11.25	14.6	7.13	9.15	5.67	10.48	0
10	10.4	0.56	0.64	0.7	0.73	0.76	0.78	0.82
		11.14	14.65	13.06	13.73	6.22	10.62	0
11	13.8	0.61	0.68	0.73	0.76	0.78	0.8	0.83
		17.04	22.69	16.4	12.41	5.17	6.41	0
12	17.3	0.66	0.74	0.76	0.8	0.81	0.83	0.84
		0	0	0	0	0	0	0
13	20.8	0.72	0.77	0.8	0.83	0.85	0.85	0.86
		0	0	0	0	0	0	0

FIGURE 6 A sample computer print-out of the numerical analysis of the cytoplasmic diffusion coefficient for the cell shown in Fig. 3*b* and the profiles in Fig. 4.

Measurements of Cytoplasmic Diffusion Constants

The average value measured for the cytoplasmic diffusion constant for FITC-BSA in the sea urchin egg was $D^{25^\circ}_{BSA} = 8.6 \pm 2 \times 10^{-8}$ cm²/s (number of samples, $n = 5$). For DTAF-tubulin, the average value of $D^{25^\circ}_{tub} = 5.9 \pm 2.2 \times 10^{-8}$ cm²/s ($n = 11$). Similar values of $D^{25^\circ}_{tub}$ were obtained for unfertilized and fertilized eggs, although the average value for unfertilized eggs, 4.7×10^{-8} cm²/s ($n = 4$) was noticeably slower than for first mitotic embryos, 6.8×10^{-8} cm²/s ($n = 7$).

Analysis of fluorescence recovery profiles for families of densitometric scans through the center of bleached regions in orthogonal directions gave the same average value of D, within the accuracy of the method (data not shown).

DISCUSSION

We have described a new way to measure diffusion coefficients of fluorescent molecules in cells and have applied the

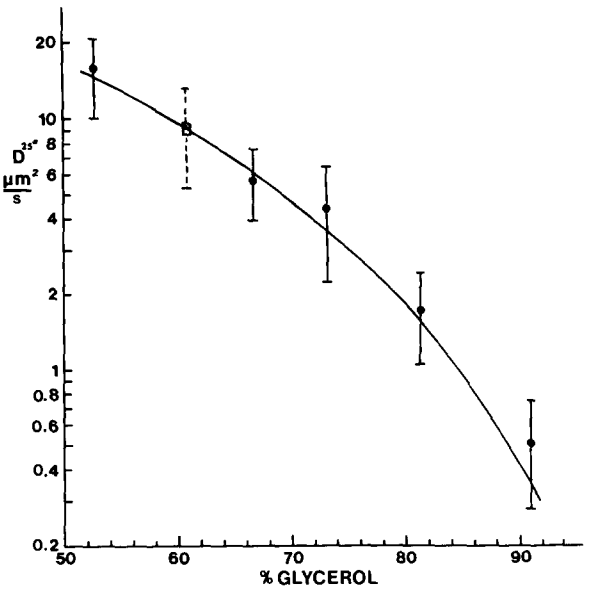

FIGURE 7 Measurements of the diffusion coefficient (D) of BSA in various glycerol-H_2O mixtures (●) compared with values calculated (solid line) from the Stokes'-Einstein equation and the viscosity of the mixtures estimated for 25°C as described in the text. The diffusion coefficient measured for FITC-BSA in the sea urchin cytoplasm is also plotted (B). Data represent average values and average standard deviations (see Fig. 6) of measurements obtained from six experiments for each viscosity.

method to sea urchin zygotes to measure the diffusion coefficient (D) of tubulin and BSA in vivo. Our approach to measuring D by video image analysis of FRAP (video FRAP) has two significant advantages. The values of D calculated do not depend critically on the initial profile of fluorescence after bleaching or on the duration of the bleach relative to the diffusion rate. Both of these boundary conditions are significant constraints on the accuracy of the standard photometric methods for determining D from the rate of redistribution of fluorescence after photobleaching, integrated throughout a bleached region (14, 15). Further, while our calculation of D is based on the assumption of cylindrical symmetry in the bleached region, a slightly asymmetrical bleaching beam yielded the same value of D when scanned in orthogonal directions.

Measurement of tracer diffusion coefficients by the analysis described here is limited to the diffusion of a single component which strictly follows Fick's Law. Multiple components or flow would complicate the analysis (13, 14). It is difficult to measure a small percentage (5%) of immobile fluorescent analog. Another disadvantage of our method are the limit on accuracy imposed by the sensitivity and signal-to-noise characteristics of the low light-level video camera, the photobleaching of the fluorochrome during photographic recording intervals, and the data acquisition rate. These disadvantages were not significant for measurement of the tracer diffusion coefficients of tubulin and BSA in the large cells of the sea urchin egg and first-division embryos (vol = 80 pl, 115 μm diam). In these cells, a low-magnification objective with relatively small numerical aperture (×25/NA = 0.5) gave sufficient resolution and illumination intensity. The epi-illumination intensities required to give usable images for a 0.5-s exposure did not significantly bleach the total cell fluorescence during the accumulated photographic exposures required to track the recovery of fluorescence after photobleaching. In the experiments reported here, the rate of data acquisition is limited by the 0.5-s photographic exposure interval and the size of the bleached region. The exposure interval was chosen as the best compromise between maximizing image quality, through video frame averaging, and maximizing the rate of data acquisition. The beam diameter of 13 ± 1 μm was a compromise between maximizing the spatial resolution in fluorescence recovery profiles and minimizing the percentage of total cell fluorescence bleached (estimated to be ~10% on the basis of total egg fluorescence before and after our experiments). Under these conditions, the accuracy of the recovery profile image analysis method is comparable to the accuracy of the standard photometric technique (15, 16, 25, 27, 28).

Application of our method for measurement of diffusion coefficients to small specimens and specimen regions that contain lesser total amounts of fluorochrome must be done with care. Higher-magnification objectives with greater numerical apertures will be needed for higher resolution video images; higher epi-illumination intensities will be required for usable video images. The higher epi-illumination intensities could produce significant bleaching of the fluorescent probe during the photographic exposure necessary for image averaging to produce usable image quality.

Experimental and theoretical aspects of photometric measurement of D by analysis of FRAP are well established (13–15). Values of D measured by the video FRAP technique described here should be identical to values measured by the photometric technique. As an additional test of the accuracy of the video-image analysis method, the diffusion constant for FITC-BSA in unfertilized eggs of *L. variegatus* was measured using photomultiplier FRAP instrumentation kindly provided by Ken Jacobson (University of North Carolina) (15, 16, 27). A value of $D_{BSA} = 9.7 \pm 0.84 \times 10^{-8}$ cm^2/s ($n = 9$) was obtained using a ×10/NA = 0.25 objective (Wadsworth, P., E. D. Salmon, and K. Jacobson, unpublished results). This value is nearly identical to the value measured here ($8.6 \pm 2.0 \times 10^{-8}$ cm^2/s) and substantiates our contention that the mobility of fluorescent molecules can be analyzed by the video FRAP method described here. Comparison of the experimental data to the theoretical curve in Fig. 7 indicates that our video FRAP measurements of tracer diffusion coefficient may overestimate the actual value by 10–20% in the range of $2.5–15.0 \times 10^{-8}$ cm^2/s. This overestimation may be due to the contribution of axial diffusion, which we have neglected in our analysis scheme.

Our measurements of D for FITC-BSA in cytoplasm suggest that the cytoplasmic viscosity of sea urchin eggs and embryos is about eight times the viscosity of water, based on the ratio of D in sea urchin cell cytoplasm ($8.6 \pm 2 \times 10^{-8}$ cm^2/s) and in water (68×10^{-8} cm^2/s) compared by Eq. 5. The Stokes'-Einstein equation predicts that a diffusion coefficient will vary with the cube root of the particle molecular weight (Eqs. 5 and 6). The diffusion coefficient determined for DTAF-tubulin in the sea urchin cell cytoplasm is $5.9 \pm 2.2 \times 10^{-8}$ cm^2/s, ~70% of the value for FITC-BSA. Eq. 6 predicts a molecular weight for DTAF-tubulin consistent with its being a freely diffusable dimer or small oligomer in sea urchin cytoplasm. Our DTAF-tubulin is competent to polymerize both in vitro (19) and in vivo (29, 30). One can even see evidence for microtubule assembly in Fig. 3*b* where a spindle is viewed end-on as a fluorescent zone brighter than the rest of the cytoplasm. However, microtubules are not observed in

TABLE I

Cytoplasmic Diffusion Coefficients of Globular Protein

Analog	M_r	$D \times 10^8$ cm²/s	T (°C)	Cell type or in vitro buffer
fl-IgG	160,000	0.8–1.1	22	BG-9 human fibroblasts (27)
fl-BSA	68,000	0.9–1.1	22	BG-9 human fibroblasts (27)
fl-BSA	68,000	1.5–2.1	37	BG-9 human fibroblasts (27)
Rh or fl-BSA	68,000	0.5–0.7	37	Embryonic chicken gizzard (28)
Rh-IgG	160,000	0.53–0.73	37	Embryonic chicken gizzard (28)
Rh-G-Actin	43,000	0.15–0.35	37	Embryonic chicken gizzard (28)
fl-BSA	68,000	33–46	25	*A. proteus* cytoplasm (25)
fl-Ovalbumin	45,000	22–53	25	*A. proteus* cytoplasm (25)
fl-G-Actin	43,000	11–25	25	*A. proteus* cytoplasm (25)
fl-Tubulin	110,000	4–10	25	*L. variegatus* cytoplasm*
fl-BSA	68,000	6–12	25	*L. variegatus* cytoplasm*
fl-Ovalbumin	45,000	3.2–3.5	25	J 744.1 microphage-like cells (25)
fl-BSA	68,000	68	25	Buffer (24, 25)
fl-Ovalbumin	45,000	89	25	Buffer (25)
fl-G-Actin	43,000	92	25	Buffer (25)
fl-Tubulin	110,000	56	25	Buffer (25)‡

Abbreviations: fl, fluorescein; Rh, rhodamine.

* This report.

‡ Calculated from Eq. 12 using $D^{20°}_{BSA}$.

the cytoplasm of unfertilized sea urchin eggs nor outside the spindle region in embryos at metaphase. These observations suggest that, when tubulin is not assembled in microtubules, it is not tightly bound to other immobile structural components of the sea urchin cytoplasm. Further experiments are required to rule out the possibility of active transport of large tubulin aggregates.

Table I lists published diffusion coefficients that have been measured for fluorescently tagged globular proteins in buffers and in the cytoplasms of several different cell types. It is clear from a comparison of the values measured for BSA that the apparent cytoplasmic viscosity for this globular protein depends significantly on the cell type used: 33–46 $\times 10^{-8}$ cm²/s for ameba; 6–12 $\times 10^{-8}$ cm²/s for sea urchin eggs and embryos; 0.9–1.1 $\times 10^{-8}$ cm²/s for human fibroblasts; and 0.5–0.7 $\times 10^{-8}$ cm²/s for chicken gizzard culture cells, all at comparable temperatures. Comparison, where possible, between the diffusion constants for other globular molecules shows a similar dependence on cell type. The origins of these differences are not yet known. They could depend on variations in the cytoplasmic rigidity and, hence, on the extent of assembly and the density of the cytoskeleton of the cell and microtrabecular lattice in different cell types (25, 27). It is therefore not possible at this time to predict the value of diffusion coefficients in one cell based upon measurements obtained from another cell type.

This work was performed in the laboratory of J. R. McIntosh while E. D. Salmon was there on sabbatical leave. The latter wishes to thank the former for an enjoyable and productive stay in his lab. We are grateful to Ken Jacobson, Pat Wadsworth, and Lans Taylor for their superb advice and stimulating discussions. Ken Jacobson also generously provided both his time and equipment so we could check our results using his photobleaching methods. Thanks also to Nancy Salmon for her usual excellent editorial assistance. We appreciate the generous loan of lasers from the following institutions: a model 136 argon laser from Spectra-Physics, Mountain View, CA; a model 1 argon laser from Lexel, Inc., Fort Worth, TX; and a Liconix model 4050 He-Cd laser from the San Francisco Laser Center, Department of Chemistry, University of California, Berkeley.

This research was supported by grants GM-24364 to Dr. Salmon and GM-31213 to Dr. McIntosh from the National Institutes of Health.

Received for publication 16 March 1984, and in revised form 6 August 1984.

REFERENCES

1. Inoué, S. 1981. Cell division and the mitotic spindle. *J. Cell Biol.* 91 (No. 3, Pt. 2):131s–147s.
2. McIntosh, J. R. 1979. Cell division. *In* Microtubules. K. Roberts and J. S. Hyams, editors. Academic Press, Inc., New York. 428–441.
3. Margolis, R. L., and L. Wilson. 1981. Microtubule treadmills—possible molecular machinery. *Nature (Lond.).* 293:705–711.
4. Salmon, E. D. 1975. Spindle microtubules: thermodynamics of in vivo assembly and role in chromosome movement. *Ann. N. Y. Acad. Sci.* 253:383–406.
5. De Brabander, M., G. Geuens, R. Nuydens, R. Willebrods, and J. DeMey. 1981. Microtubule assembly in living cells after release from nocodazole block. *Cell Biol. Int. Rep.* 5:913–920.
6. Hill, T. L., and M. W. Kirschner. 1982. Regulation of microtubule and actin filament assembly-disassembly. *Int. Rev. Cytol.* 84:185–234.
7. Mitchison, T. J., and M. W. Kirschner. 1984. Dynamic instability of microtubule growth. *Nature (Lond.).* In press.
8. Salmon, E. D., M. McKeel, and T. Hays. 1984. The rapid rate of tubulin dissociation from microtubules in the mitotic spindle in vivo measured by blocking polymerization with colchicine. *J. Cell. Biol.* 99:1066–1075.
9. Koren, R., and G. G. Hammer. 1976. A kinetic study of protein–protein interactions. *Biochemistry.* 15:1165–1171.
10. Setlow, R. B., and E. C. Pollard. 1962. Molecular Biophysics. Addison-Wesley, Reading, MA. 498–504.
11. Taylor, D. L., P. A. Amato, K. Luby-Phelps, and P. McNeil. 1984. Fluorescent analog cytochemistry. *Trends Biochem. Sci.* 9:88–91.
12. Kreis, T., and W. Birchmeier. 1982. Microinjection of fluorescently labeled proteins into living cells with emphasis on cytoskeletal proteins. *Int. Rev. Cytol.* 75:209–227.
13. Jacobson, K., E. Elson, D. Koppel, and W. Webb. 1983. International workshop on the application of fluorescence photobleaching techniques to problems in cell biology. *Fed. Proc.* 42:72–79.
14. Axelrod, D., D. E. Koppel, J. Schlessinger, E. Elson, and W. W. Webb. 1976. Mobility measurement by analysis of fluorescence photobleaching recovery kinetics. *Biophys. J.* 16:1055–1069.
15. Jacobson, K., Z. Dersko, E-S. Wu, Y. Hou, and G. Poste. 1976. Measurement of the lateral mobility of cell surface components in single, living cells by fluorescence recovery after photobleaching. *J. Supramol. Struct.* 5:565–576.
16. Jacobson, K., E-S. Wu, and G. Poste. 1976. Measurement of the translational mobility of concanavalin A in glycerol-saline solutions and on the cell surface by fluorescence recovery after photobleaching. *Biochim. Biophys. Acta.* 433:215–222.
17. Weingarten, M. D., M. M. Suter, D. R. Littman, and M. W. Kirschner. 1974. Properties of the depolymerization products of microtubules from mammalian brain. *Biochemistry.* 13:5529–5537.
18. Keith, C. H., J. R. Feramisco, and M. Shelanski. 1981. Direct visualization of fluorescein-labeled microtubules in vitro and in microinjected fibroblasts. *J. Cell Biol.* 88:234–240.
19. Leslie, R., W. M. Saxton, B. Neighbors, T. Mitchison, E. D. Salmon, and J. R. McIntosh. 1983. Assembly properties of fluorescein-labeled tubulin in vitro before and after fluorescence bleaching. *J. Cell Biol.* 99:2146–2156.
20. Kiehart, D. 1981. Studies on the in vivo sensitivity of spindle microtubules to calcium ions and evidence for a vesicular calcium-sequestering system. *J. Cell Biol.* 88:604–617.
21. Izant, J. G., J. A. Weatherbee, and J. R. McIntosh. 1982. A microtubule-associated protein antigen unique to mitotic spindle microtubules in PtK_1 cells. *J. Cell Biol.* 96:424–434.
22. Crank, J. 1956. The Mathematics of Diffusion. Clarendon Press, Oxford. 347 pp.
23. Carslaw, H. W., and J. C. Jaeger. 1960. Conduction of Heat in Solids, 2nd Edition. Clarendon Press, Oxford. 510 pp.
24. Barisas, B. G., and M. D. Leuther. 1979. Fluorescence photobleaching recovery measurement of protein absolute diffusion constants. *Biophys. Chem.* 10:221–229.
25. Wang, Y-L., F. Lanni, P. L. McNeil, B. R. Ware, and D. L. Taylor. 1982. Mobility of cytoplasmic and membrane-associated actin in living cells. *Proc. Natl. Acad. Sci. USA.* 79:4660–4664.
26. Handbook of Chemistry and Physics, 57th Edition. D210 Chemical Rubber Co., Cleveland, OH.
27. Wojcieszyn, J. W., R. A. Schlegel, E.-S. Wu, and K. A. Jacobson. 1981. Diffusion of injected macromolecules within the cytoplasm of living cells. *Proc. Natl. Acad. Sci. USA.* 78:4407–4410.
28. Kreis, T. E., B. Geiger, and J. Schlessinger. 1982. Mobility of microinjected rhodamine actin within living chicken gizzard cells determined by fluorescence photobleaching recovery. *Cell.* 29:835–845.
29. Salmon, E. D., R. Leslie, W. M. Saxton, M. L. Karow and J. R. McIntosh. 1983. Spindle microtubule dynamics in sea urchin embryos. Analysis using a fluorescein-labeled tubulin and measurements of fluorescence redistribution after photobleaching. *J. Cell Biol.* 99:000–000.
30. Saxton, W. M., R. J. Leslie, E. D. Salmon, M. Zavortink and J. R. McIntosh. 1983. Tubulin dynamics in cultured mammalian cells. *J. Cell Biol.* 99:000–000.